Two-dimensional weak localization in partially graphitic carbons

V. Bayot, L. Piraux, J.-P. Michenaud, and J.-P. Issi
Unité de Physico-Chimie et de Physique des Matériaux, Département des Sciences des Matériaux et des Procédés, Université Catholique de Louvain, place Croix du Sud, 1 B-1348 Louvain-la-Neuve, Belgium

M. Lelaurain
Laboratoire de Chimie du Solide Minéral, L.A. 158, Service de Chimie Minérale Appliquée, Université de Nancy I, Boîte Postale 239, 54506 Vandoeuvre-les-Nancy CEDEX, France

A. Moore
Union Carbide Corporation, Parma Technical Center, P.O. Box 6116, Cleveland, Ohio 44101
(Received 13 February 1990)

The weak-localization phenomenon for two-dimensional (2D) electronic systems is invoked to explain the negative magnetoresistance as well as the low-temperature dependence of the resistivity of pyrocarbon samples heat treated between 2000 and 2600 °C. The 2D character is found to originate from the random stacking of the graphene layers (turbostratic structure) characteristic of pregraphitic carbon materials. For a heat-treatment temperature (HTT) lower than 2200 °C, x-ray analysis reveals that the structure is almost turbostratic, while the material exhibits a pronounced negative magnetoresistance. For higher HTT, 3D order typical of crystalline graphite increases, leading to a 2D-to-3D crossover and to a vanishing negative magnetoresistance.

I. INTRODUCTION

Weak localization is a general phenomenon which occurs whenever waves propagate in a disordered medium.[1–3] In electronic systems, it originates from interference effects between elastically scattered partial carrier waves, while in the Boltzmann approximation they are not taken into account.[2] These interferences are constructive in the backward direction of propagation, resulting in a backscattering probability enhancement. Therefore, it leads to an additional contribution to the resistivity superimposed to the classical Boltzmann contribution.

Since inelastic scattering processes due to electron-phonon or electron-electron interactions destroy the phase coherence between carrier waves, weak localization is essentially a low temperature phenomenon. Also, an external applied magnetic field suppresses the phase coherence.[2,4] In the absence of spin-dependent scattering mechanisms, the two main features of the weak-localization effect for two-dimensional (2D) systems are a logarithmic increase of the resistivity at low temperature and a negative magnetoresistance.[2,4,5] The theory has been extended to take into account other scattering mechanisms, namely the spin-orbit coupling which produces an antilocalization effect and the scattering by magnetic impurities which produces a saturation of the additional resistivity at low temperature.[2,4] The weak-localization effect occurs whatever the dimensionality of the electronic system, but is much more pronounced for 2D systems than for 3D systems.[3] It has been observed in many 2D electronic systems such as thin metallic films[2] and heterostructures.[5]

This model has also been applied with success to explain low-temperature electronic transport properties in acceptor graphite intercalation compounds (GIC's).[6–8] In these materials, the 2D character of the electronic system is obvious since the intercalated species play the role of barriers for the motion of the carriers which remain confined in the graphene layer planes.[9]

Well before the weak-localization effect was predicted and experimentally observed in many electronic systems, a negative magnetoresistance had already been reported in disordered pregraphitic materials by Mrozowski and Chaberski.[10] This unusual phenomenon was found to be a general feature of poorly graphitized samples.[11–13] Pregraphitic materials are characterized by a turbostratic structure consisting of a random stacking of graphene layer planes, in contrast to graphite crystals in which those planes are stacked in the well known $ABAB\ldots$ sequence.[14,15] Structural analysis showed that the parameter which is mainly responsible for the occurrence of the negative magnetoresistance is the degree of three-dimensional (3D) ordering of the graphene planes. Increasing the heat-treatment temperature (HTT) both increases the 3D order and eliminates the negative magnetoresistance.[11,12]

In 1969, Yazawa[16] proposed a model based on the increase of the carrier density with increasing magnetic field to explain the negative magnetoresistance. Ten years latter, Bright showed that this model was not complete and proposed a more detailed theory.[17] Owing to the turbostratic structure, he used the 2D band model developed from the results of Wallace[18] and McClure[19] for the magnetic field quantization of the density of states DOS in discrete Landau levels. Disorder-induced

broadening was invoked to explain the absence of Shubnikov–de Haas oscillations. Finally, Bright showed that the DOS, and consequently the carrier density, increases under an applied magnetic field. However, recent works[20,21] showed that the Bright model was unable to explain both the temperature dependence of the magnetoresistance and the high-field behavior. It is worth noting that the Bright model also leans on the 2D character of pregraphitic carbon materials to explain the negative magnetoresistance. In that case, the negative magnetoresistance originates from a 2D band-structure model rather than from a 2D diffusion of carriers.[22] In contrast, for a given dimensionality, the weak-localization phenomenon is not affected by the details of the band model considered, so that it appears as a more universal effect.

Using high-resolution measurements, we recently demonstrated that the low-temperature dependence of the zero-magnetic-field resistivity of pristine carbon fibers, which showed negative magnetoresistance, was also anomalous:[22] the resistivity exhibited a negative temperature coefficient down to 1.7 K. It was shown[22] that this result cannot be explained at low temperature by a thermal excitation of carriers in the framework of the simple two-band (STB) model.[15,23]

According to the similar features of the negative magnetoresistance observed in disordered pregraphitic materials and in low-stage acceptor GIC's, we used the same theory to explain this phenomenon in both systems. We showed that the weak-localization theory in the 2D regime might explain the negative magnetoresistance as well as the negative temperature coefficient of the resistivity observed at low temperature in pregraphitic carbon fibers.[22]

But in pristine pregraphitic materials the origin of the 2D character is less obvious than in acceptor GIC's. We are thus interested to find the origin of the 2D character of pregraphitic carbons within the framework of the weak-localization phenomenon: a two-dimensional elastic diffusive motion of the carriers.

Since, as stated above, the heat-treatment temperature appears to be the main parameter which governs the degree of 3D ordering in pregraphitic materials, we have performed magnetoresistance and x-ray measurements on a set of pyrocarbon samples heat treated at different temperatures in the range 2000 to 2600 °C where all samples exhibit negative magnetoresistances.

In this paper, it is clearly shown from the x-ray analysis that a transition from turbostratic to graphitic structure arises when the HTT exceeds 2300 °C, as already observed in other works.[11,12,14,24,25] The magnetoresistance data are analyzed in the framework of the weak-localization theory and the values of the obtained parameters are discussed. It appears that the 2D character of pregraphitic materials originates from the turbostratic structure, and that the temperature dependence of the resistivity is the sum of the Boltzmann and the weak-localization contributions. Finally, we show that the diffusion of the carriers by magnetic impurities plays an important role in the negative magnetoresistance effect at low temperature.

II. EXPERIMENT

The pyrocarbon material for the measurements described below was prepared by pyrolyzing methane on graphite substrates in a laboratory induction furnance at 1680 °C and 0.5 Torr. This pyrocarbon had a mosaic spread, i.e., full width at half maximum of the (002) orientation distribution, of 45°. Turbostratic structure was indicated by measured interlayer spacing of 3.43 Å, which is 2% larger than the interlayer spacing of ideal graphite. The specific gravity was 2.15 g/cm^3.

Portions of the above pyrocarbon sample were heat treated in a laboratory graphite induction furnance in one atmosphere of argon at temperatures up to 2800 °C. Separate samples were heated for 30 min periods at 100 °C temperature intervals over the range 1800–2800 °C. Heating and cooling time was kept to a practical minimum. Samples were heated to 1700 °C in 20–25 min. Above 1700 °C, the heating rate was 25–40 °C/min, depending on the final temperature. The cooling rate to 1700 °C was similar to the heating rate above 1700 °C.

Samples of $10\times3\times0.2$ mm^3 in dimensions were used for resistivity and magnetoresistance measurements. A conventional dc four-probe method was used with silver paste contacts. A cryostat was used for measurements in the temperature range between 1.7 and 300 K. Magnetic fields up to 1 T perpendicular to the sample surface were provided by means of a classical electromagnet. The current flowing in the sample was provided by a high stability current source (Keithley K224) and the power dissipated was kept sufficiently low to avoid self-heating. The voltage was measured accurately by means of a Keithley K181 nanovoltmeter which could resolve 10^{-8} V, while the signal allowed a resolution of a few parts in 10^5. To avoid spurious voltage due to transverse effects, we averaged the values of the magnetoresistance found by reversing both current and magnetic field directions.

The structural characterization of the samples involved the following steps: (i) measurement of the mosaic spread about the c axis, (ii) recording of the $0\,0\,l$ and $h\,k\,0$ reflections, and (iii) determination of the distribution of intensity along a given $h\,k\,l$ (primarily the $1\,0\,l$).[26]

The diffraction setup consisted of a 1-kW molybdenum source, a quartz monochromator (for $K\alpha_1$ selection), and a vertical axis goniometer, equipped with a scintillation counter, in the center of which was placed the sample holder which allowed all measurements to be made on a single sample ($10\times1\times0.2$ mm^3). The measurement was carried out by transmission. For the precise determination of interplanar distances (d_i) based on the $0\,0\,l$ reflections, diamond powder was used as a standard.

III. RESULTS

A. X-ray analysis

In Table I we report the experimental values of mosaic spread and interplanar distance, d_i, based respectively on the 004 reflection and the position of the center of gravity of the 002, 004, and 006 peaks.

TABLE I. Parameters found by the x-ray analysis. d_i is the mean interlayer spacing, p the order parameter defined in the text, and the mosaic spread is also defined in the text.

HTT (°C)	d_i (Å)	p	Mosaic spread (deg)
2000	3.423	0.90	33
2100	3.421	0.88	40
2200	3.405	0.77	36
2300	3.388	0.63	38
2400	3.372	0.46	44
2500	3.357	0.2	27
2600	3.355	0.1	21

Figure 1 shows the existence of three distinct regions according to the temperature of heat treatment.

(i) for HTT ranging between 1700 and 2100°C, $d_i \cong 3.42$ Å, which is typical of a turbostratic structure.

(ii) For $T_{HT} \geq 2500$ °C, the dimensions of the ordered domains in the c direction increase while the interplanar distance is very close to that of graphite.

(iii) Finally, for $2200 \leq T_{HT} \leq 2400$ °C, the HTT affects drastically the mean interlayer spacing, showing that graphitization occurs.

As will be seen in the following paragraphs, the galvanomagnetic properties are closely correlated to these structural modifications. A complete analysis of the crystallographic data, including the $h\,k\,l$ profiles, will be presented in a next paper.

We introduce the structural parameter p as the probability of finding two neighboring graphene layers of a partially turbostratic sample in a randomly stacked configuration. As a consequence, $1-p$ is the probability of finding two layers in an AB stacking configuration characteristic of the graphite crystal. When $p=1$, the sample is fully turbostratic, while for a perfect 3D single crystal, $p=0$.[14]

A relation between the parameter p and the value of the mean interlayer spacing d_i, as determined by x-ray analysis, has been previously established[14] and later confirmed:[27]

$$d_i = 3.354 + 0.086p^2 , \quad (1)$$

where d_i is expressed in angstroms. The values of the parameter p found for our samples using relation (1) are also given in Table I.

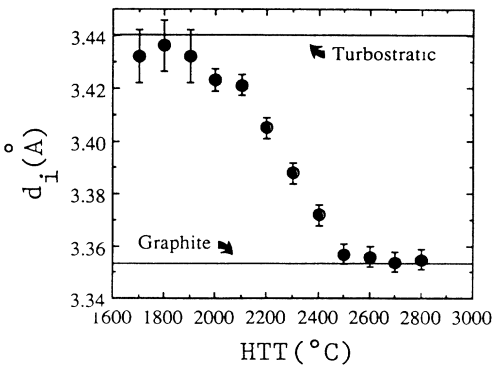

FIG. 1. Effect of the heat-treatment temperature HTT on the mean interlayer spacing, d_i. The turbostratic- ($d_i = 3.44$ Å) to-graphitic ($d_i = 3.354$ Å) transition occurs mainly for $2200 \leq T_{HT} \leq 2400$ °C.

B. Resistivity and magnetoresistance

The temperature dependence of the resistivity of selected samples heat treated at 2000, 2300, and 2600 °C between 1.7 and 300 K are presented in Fig. 2(a). In Fig. 2(b), the low-temperature behavior is presented in more detail. The liquid-helium temperature resistivity values, ρ(4.2 K), as well as the residual resistance ratio [ρ(300 K)/ρ(4.2 K)], are given in Table II for all the samples studied.

We see that, for each sample, the resistivity exhibits a negative temperature coefficient down to the lowest temperature investigated. This behavior has also been ob-

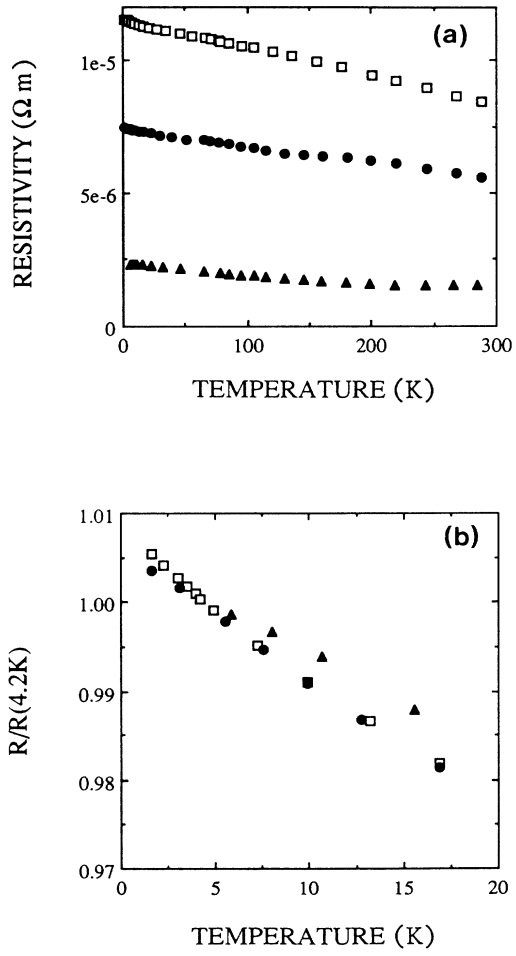

FIG. 2. Temperature dependence of the resistivity of the samples heat treated at 2000, (□), 2300, (●), and 2600 °C (▲). Over the whole temperature range investigated, the resistivity increases monotonically as the temperature is decreased (a). The low temperature behavior (b) cannot be understood by simply invoking a thermal excitation of carriers.

TABLE II. Zero-magnetic-field resistivity and residual resistance ratio.

HTT (°C)	ρ(4.2 K) (10^{-6} Ω m)	ρ(300 K)/ρ(4.2 K)
2000	11.5	0.73
2100	9.5	0.70
2200	8.5	0.72
2300	7.4	0.75
2400	6.4	0.62
2500	3.3	0.66
2600	2.3	0.65

served in pregraphitic carbons fibers[22] and in pyrocarbons[28] which all show a negative magnetoresistance.

The magnetoresistance data as a function of magnetic field at various temperatures are presented in Fig. 3 over the whole magnetic field range investigated. The magnetoresistance is negative at low temperature and at low magnetic field. As the temperature rises, the magnetoresistance becomes less and less negative, and above a given temperature, which is sample dependent, the magnetoresistance becomes definitively positive. This behavior is similar to that observed in pregraphitic carbon fibers.[22]

The magnetoresistance behavior at 4.2 K for the samples of various values of HTT is summarized in Fig. 4. The amplitude of the negative magnetoresistance is comparable for the samples heat treated at 2000, 2100, and 2200 °C. When the HTT rises above 2300 °C, the negative component of the magnetoresistance vanishes drastically and becomes very small for $T_{HT}=2600$ °C. Simultaneously, the positive component of the magnetoresistance becomes more and more important. This general behavior is in agreement with results presented elsewhere.[11]

IV. DISCUSSION

A. Theoretical background

In the framework of the weak-localization theory, the correction to the sheet conductance G as the magnetic field H is applied perpendicular to the 2D electronic system is given by[4,29]

$$G(H,T)=G_0+\frac{e^2}{2\pi^2\hbar}\left[-\Psi\left(\frac{1}{2}+\frac{H_1}{H}\right)+\tfrac{3}{2}\Psi\left(\frac{1}{2}+\frac{H_2(T)}{H}\right)-\tfrac{1}{2}\Psi\left(\frac{1}{2}+\frac{H_3(T)}{H}\right)\right], \quad (2)$$

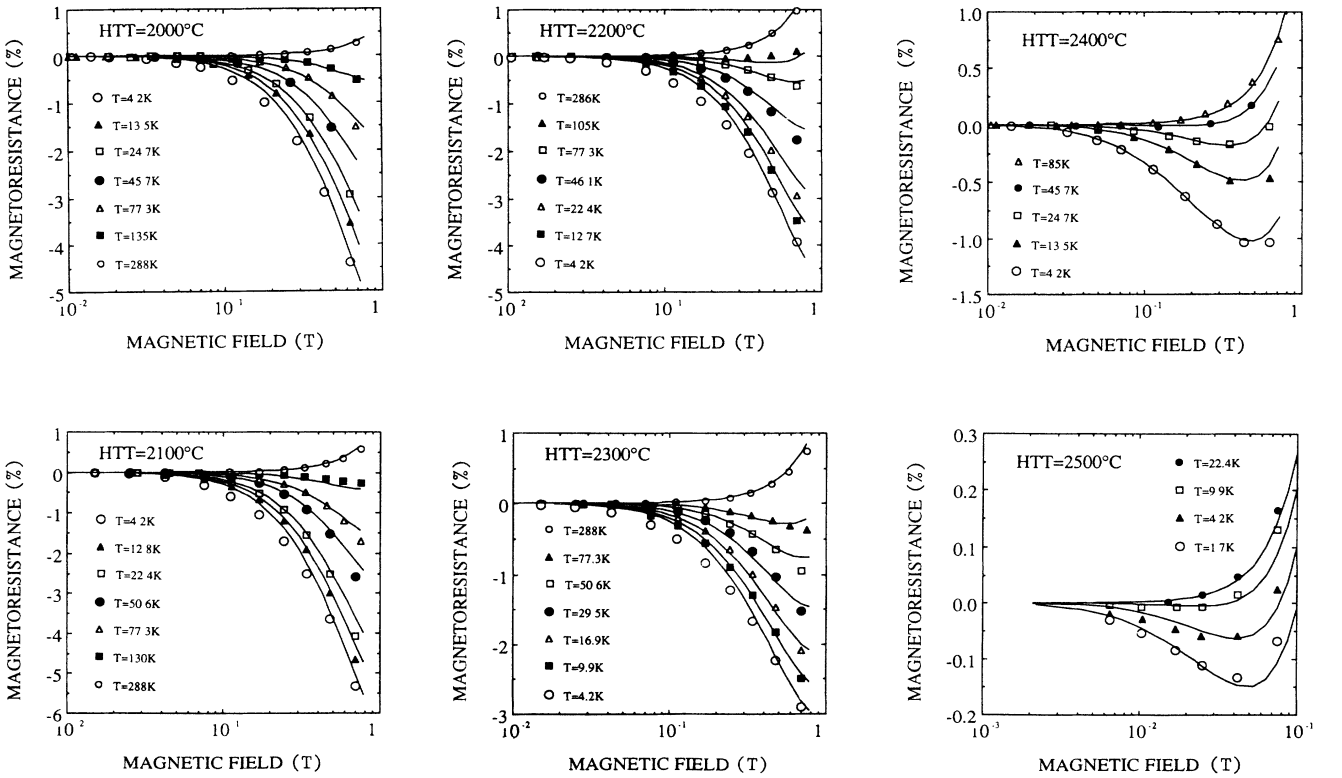

FIG. 3. Magnetoresistance (%) as a function of magnetic field at various temperatures as indicated, for various samples (each shown separately) with heat-treatment temperature between 2000 and 2500 °C. The symbols represent experimental data, while the curves result from the best-fit calculations. For all the samples, the magnetoresistance becomes less and less negative as the temperature rises. Above a given temperature, which is sample dependent, the magnetoresistance becomes definitively positive. The relations of the weak-localization theory reproduce fairly well the magnetoresistance data over a wide range of magnetic field and temperature.

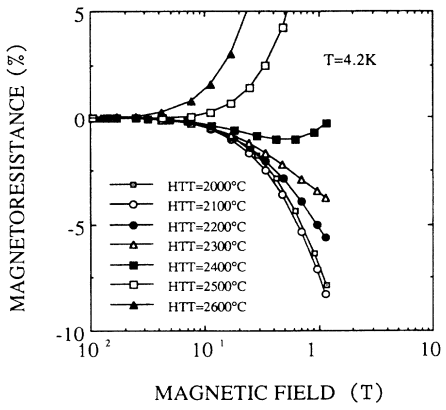

FIG. 4. Magnetoresistance (%) at $T=4.2$ K as a function of the magnetic field for the samples heat treated at the indicated temperatures. When the HTT is raised above 2300 °C, the negative component of the magnetoresistance progressively vanishes.

where G_0 is the sheet conductance as calculated in the classical Boltzmann formulation of the transport theory. In the special case of a film considered as a quasi-2D system, the sheet conductance is the product of the 3D conductivity by the thickness of the film. In Eq. (2), Ψ is the digamma function and H_1, $H_2(T)$, and $H_3(T)$ are defined by

$$H_1=H_0+H_{\text{s.o.}}+H_s \ ,$$

$$H_2(T)=H_i(T)+\tfrac{4}{3}H_{\text{s.o.}}+\tfrac{2}{3}H_s \ ,$$

$$H_3(T)=H_i(T)+2H_s \ ,$$

where the quantities

$$H_k=\frac{\hbar}{4eD\tau_k} \quad (k=0,i,s,\text{s.o.}) \tag{3}$$

represent the characteristic magnetic fields associated with the scattering mechanism, k: elastic scattering (0), inelastic scattering (i), magnetic impurity scattering (s), or spin-orbit coupling (s.o.); τ_k is the relaxation time corresponding to the scattering type "k" and D is the diffusion constant:

$$D=\tfrac{1}{2}v_F^2\tau_0 \ , \tag{4}$$

where v_F is the Fermi velocity.

In the limit of zero magnetic field, Eq. (2) becomes

$$G(0,T)=G_0+\frac{e^2}{2\pi^2\hbar}\ln\left[\frac{H_2^{3/2}}{H_1H_3^{1/2}}\right] . \tag{5}$$

For convenience, we discuss our results in terms of the magnetoresistance $\Delta R/R$ rather than in terms of the magnetoconductance $\Delta G/G$, where $\Delta G=G(H,T)-G(0,T)$. Since $\Delta G/G \ll 1$, we have $\Delta R/R \cong -\Delta G/G$. Also, we introduce the sheet resistance $R_\square=1/G_0$.

Comparing experimental data with the above theoretical relations, it is, in principle, possible to determine the values of the parameters $R_\square$, H_0, H_s, $H_{\text{s.o.}}$ and H_i for a given sample and at a given temperature. These parameters are directly related to the relaxation times of the corresponding scattering mechanisms. Therefore, the weak-localization effect is a unique and powerful tool to investigate separately the different scattering mechanisms which, in the interpretation of a classical transport measurement, are generally masked by the dominant scattering mechanism due to lattice defects or by other temperature-dependent parameters. For example, the temperature dependence of τ_i will be determined even in the lowest temperature range where $\tau_0 \ll \tau_i$. Likewise, the scattering of carriers by magnetic impurities will be determined even when $\tau_0 \ll \tau_s$.

The analysis of the negative magnetoresistance data within the framework of the weak-localization theory is the purpose of the next section.

B. Magnetoresistance data analysis

In addition to the negative magnetoresistance due to the weak-localization effect, the so-called Lorentz-type positive magnetoresistance has to be taken into account in performing a detailed quantitative analysis of the data obtained in our samples. We make the assumption that the observed magnetoresistance can be expressed as the sum of two terms:

$$(\Delta R/R)_{\text{expt}}=(\Delta R/R)_{\text{Lorentz}}+(\Delta R/R)_{w\text{-}l} \ . \tag{6}$$

In the limit of low magnetic field, i.e., when $\mu H \ll 1$ (Refs, 24, 30, and 31),

$$(\Delta R/R)_{\text{Lorentz}} \cong (\mu H)^2 \ , \tag{7}$$

where μ is the mobility of the carriers expressed by

$$1/\mu=1/\mu_0+1/\mu_i \ ,$$

where μ_0 corresponds to defect scattering and μ_i to scattering by phonons.

Our analysis has been restricted to the temperature and magnetic field ranges where the negative component of the magnetoresistance appears clearly and where the H^2 dependence of the positive component is observed. Thus, for poorly graphitized samples, i.e., when $2000 \le T_{\text{HT}} \le 2300$ °C, the whole set of data obtained from 1.7 to 300 K was analyzed up to 0.8 T. For the samples heat treated at 2400, 2500, and 2600 °C, we restricted our analysis below 85, 22, and 8 K, and for magnetic fields lower than 0.8, 0.1, and 0.05 T, respectively. Since $\mu_i \gg \mu_0$ for all the samples in their correspondingly limited temperature range, we can reasonably assume that $\mu \cong \mu_0$.

At low temperature, no positive magnetoresistance appears in the low-magnetic-field range whatever the sample considered (Fig. 3). This means that spin-orbit coupling is negligible in our samples, i.e., $H_s \gg H_{\text{s.o.}}$. So, in the fitting procedure, we may set $H_{\text{s.o.}}=0$ at each temperature.

The temperature dependence of the negative magnetoresistance is mainly included in the parameter $H_i(T)$.

In a previous study performed on pregraphitic carbon fibers,[22] we showed that the temperature dependence of H_i is best expressed by

$$H_i = \alpha T \ . \tag{8}$$

The sheet resistance $R_\square$ is a function of both the relaxation time τ_0, which is temperature independent, and the carrier densities n and p, whose temperature dependence cannot *a prori* be neglected for our samples in the temperature range considered. The values of $R_\square$ given in Table III are those obtained in the liquid-helium temperature range. For higher temperatures, the $R_\square$ has been lowered according to the increase of the carrier density. The estimation of the temperature dependence of the carrier density will be discussed in Sec. IV C.

The influence of the mosaic spread on the observed magnetoresistance has been taken into account by means of the relations given in Appendix A.

Only four temperature-independent parameters $R_\square$, α, H_s, and μ_0 are used to fit the magnetoresistance data as a function of magnetic field and temperature for a given sample. The fit was carried out using the usual least-squares method. Both experimental results and best-fit calculations are presented in Fig. 3 and the corresponding values of the fitting parameters are given in Table III.

The values of H_0 given in Table III were roughly estimated using relations (3) and (4), taking a typical value for $v_F \approx 10^6$ m/s (Ref. 15) and the corresponding values of μ_0 for each sample. Fortunately, even a very rough estimation of H_0 would not significantly affect the values found for the other fitting parameters since the fitting calculations were performed with $H < H_0$. Indeed, when $H < H_0$ the temperature dependence of the magnetoresistance is not affected by the value of H_0.

For the samples heat treated between 2000 and 2200 °C the fitting parameters take very close values. On the other hand, for the samples heat treated at higher temperature, $R_\square$ and H_s decrease significantly, while μ_0 increases. It must be noted that these rapid changes in the parameters with HTT correspond to the HTT range where the turbostratic-to-graphitic transition occurs.

C. Temperature dependence of the resistivity

Using relation (5) and the values of the parameters given in Table III, it is possible to estimate the contribution of the weak-localization effect to the zero-magnetic-field resistivity. Subtracting this contribution from the total measured resistivity, we obtain the so-called Boltzmann contribution.

Figure 5(a) shows that the temperature dependence of the Boltzmann resistivity and of the total measured resistivity for the sample heat treated at 2000 °C are qualitatively different. The samples heat treated between 2000 and 2200 °C show a similar behavior. The low-temperature Boltzmann contribution, which is about 30% smaller than the total resistivity, is presented in more detail in Fig. 5(b). At low temperature, the resistivity increases almost linearly with the temperature. Above a given temperature, which is sample dependent, the temperature coefficient of the resistivity is reversed from positive to negative. This behavior is characteristic of well-graphitized samples when no magnetic field is applied.[24,25,30,31] The low-temperature behavior is ascribed to the decreasing mobility with rising temperature, while the high-temperature behavior results from the thermal excitation of carriers which increases the total carrier density.[25] The temperature dependence of the carrier density has been derived from the Boltzmann resistivity and used to correct the value of the sheet resistance $R_\square$ in the fitting procedure.

The Boltzmann contribution to the resistivity of the sample heat treated at 2400 °C is presented in Fig. 5(c). All the samples heat treated above 2300 °C studied here show a similar behavior. It appears that the thermal excitation of carriers becomes important at much lower temperature than for the samples heat treated at 2000, 2100, and 2200 °C.

Figure 6 includes both the Boltzmann resistivity and the total measured resistivity at $T = 4.2$ K. The magnitude of the weak-localization contribution decreases when the HTT is increased and vanishes for $T_{HT} \geq 2600$ °C.

These results provide strong support for the interpretation of the negative magnetoresistance in pregraphitic materials in terms of weak localization, since it is possible, with this model, to understand the temperature dependence of the resistivity as well.

D. Origin of the 2D character

For most of the electronic systems exhibiting 2D weak localization, the physical origin of the 2D character is relatively easy to understand. In thin metallic films, it is the sample surfaces which restrict the motion of the car-

TABLE III. Parameters found by the best-fit calculation performed on the magnetoresistance data, using relations (2) and (5)–(8).

HTT (°C)	$R_\square$ (Ω/square)	H_s (T)	α (10^{-3} T/K)	μ_0 (m^2/V s)	H_0 (T)
2000	6230	2.0×10^{-1}	1.9	0.12	4.5
2100	6970	2.0×10^{-1}	1.8	0.15	2.8
2200	6680	2.0×10^{-1}	1.9	0.18	2.1
2300	3590	1.3×10^{-1}	1.7	0.15	1.5
2400	916	3.0×10^{-2}	2.2	0.16	1.0
2500	170	3×10^{-3}	1.0	0.62	0.1
2600	30	$\approx10^{-4}$	0.2	1.17	0.05

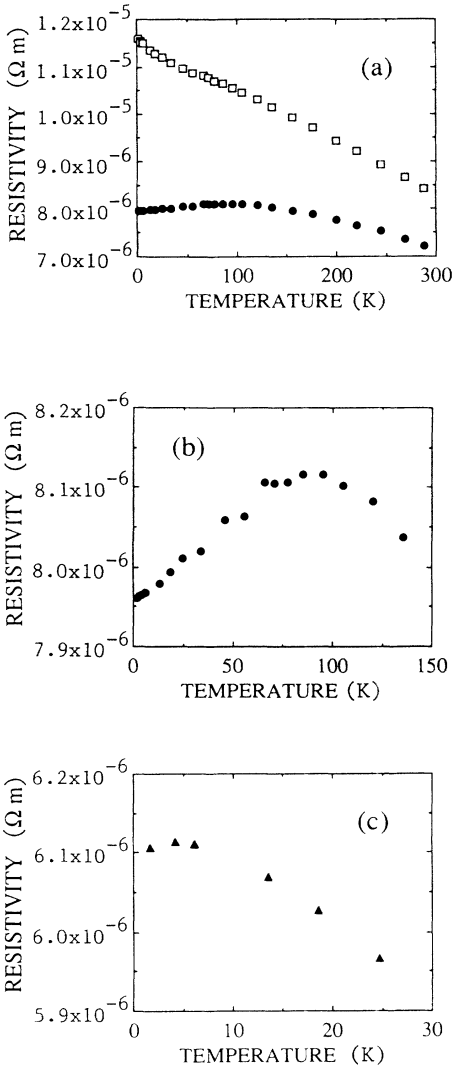

FIG. 5. Temperature dependence of the resistivity. (a) for $T_{HT}=2000\,^{\circ}C$ and for T up to 300 K: □, total measured resistivity; and ●, Boltzmann contribution to the resistivity obtained after subtraction of the weak localization contribution (see text). (b) and (c) Low-temperature Boltzmann contribution for the sample heat treated at 2000 °C (●) and 2400 °C (▲). For the latter, the thermal excitation of carriers starts to play a significant role at much lower temperature than for the former.

riers in a plane. For heterostructures and superlattices, the carriers are confined in a 2D potential well, while in acceptor GIC's the carriers are totally localized in graphene layers. In contrast, in pregraphitic materials, the origin of the 2D character is *a priori* not so obvious.

For thin metallic films as well as for superlattices, $R_{\square}$ is given by the ratio of ρ_0 and the thickness of the quasi-2D system, ξ. For inhomogeneous systems containing cracks, voids, amorphous domains, and extra-resistive boundaries, a correction coefficient $0<\lambda<1$ has to be introduced,[8,32] so that

$$\frac{\rho_0}{R_{\square}}=\xi\lambda^{-1}\,.$$

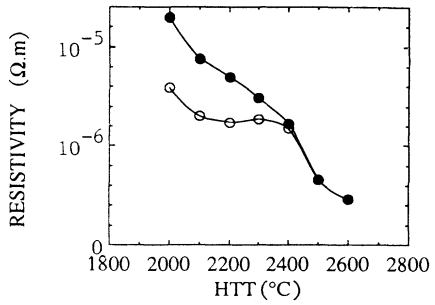

FIG. 6. Resistivity at $T=4.2$ K as a function of HTT. The difference between the total measured resistivity (●) and the Boltzmann contribution (○) is important for low values of HTT and vanishes for $T_{HT}\geq 2500\,^{\circ}C$. The solid lines are guides for the eye.

We present in Fig. 7 the HTT dependence of $\rho_0/R_{\square}$. This ratio increases drastically for $T_{HT}\geq 2300\,^{\circ}C$, suggesting a 2D-to-3D crossover as far as the 2D weak-localization phenomenon is concerned. We now try to correlate this behavior with structural modifications revealed by x-ray measurements. For that purpose, the ratio $\rho_0/R_{\square}$ is plotted against p which characterizes the degree of three-dimensional ordering (Fig. 8). It is seen that $\rho_0/R_{\square}$ exhibits approximately a p^{-2} dependence.

Negative magnetoresistance is present in turbostratic samples while it is absent in graphitic ones. Therefore, the relative amount of turbostratic layers in a sample should be of importance to determine the magnitude of this effect. The probability of finding a turbostratic graphene layer, i.e., that which is randomly stacked with respect to its two neighbors, is equal to $p*p=p^2$. The relative contribution of these layers to the total conductance of the sample is also equal to p^2. Moreover, within the framework of the weak-localization theory, the amplitude of the negative magnetoresistance is proportional to $R_{\square}$. Consequently, if we make the hypothesis that in partially turbostratic samples, only the turbostratic layers contribute to the 2D weak-localization phenomenon, we

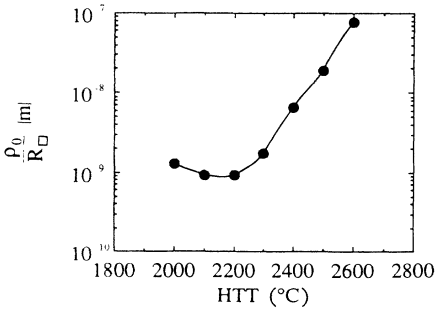

FIG. 7. Evolution of the ratio $\rho_0/R_{\square}$ with varying HTT (see text). When the HTT is raised above 2300 °C, $\rho_0/R_{\square}$ increases drastically, suggesting a 2D-to-3D crossover as far as the weak-localization phenomenon is concerned. Solid curve is guide to the eye.

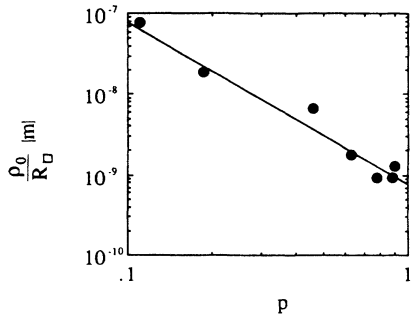

FIG. 8. Ratio $\rho_0/R_\square$ as a function of the structural parameter p which characterizes the partially graphitic state. The symbols are experimental data while the solid line corresponds to a p^{-2} dependence with $\lambda=0.5$ (see text).

find for the apparent $R_\square$ the following expression:

$$R_\square = p^2 \frac{\lambda \rho_0}{d_i} ,$$

thereby accounting for the p^{-2} dependence of $\rho_0/R_\square$.

The present model reproduces quite well the experimental values of Fig. 8 for a wide range of p and thus for very different degrees of graphitization. A reasonable value for $\lambda \approx 0.5$ is required to fit quantitatively the experimental values of $\rho_0/R_\square$ found for all the samples investigated in this study. Values for λ given in the literature are typically found between 0.1 and 1.[2,7,32]

X-ray and magnetoresistance results tend to show that partially graphitized carbon is a mixture of two phases. The first consists of well-stacked graphene planes in the *ABAB* . . . sequence characteristic of crystalline graphite, while the second consists of turbostratic layers. According to the present results, the turbostratic phase is found to be responsible for the 2D behavior in the sense of the weak localization.

E. Magnetic impurities

We now discuss the influence of the HTT on the magnetic impurity scattering time τ_s which should reflect the magnetic impurity concentration in the sample. For the estimation of the value of D, see Appendix B.

From Fig. 9, it appears that for $T_{HT} \geq 2300$ °C, τ_s increases significantly. The value of τ_s found for the sample heat treated at 2200 °C is about 2 orders of magnitude lower than that of the sample heat treated at 2500 °C. Since $1/\tau_s$ is proportional to the magnetic impurity concentration, this result is in fairly good agreement with those found by other techniques[33] which show that implanted impurities diffuse between the graphene planes and goes out of the sample for $T_{HT} \geq 2300$ °C. Moreover, iron, which is known to constitute impurities in pyrocarbon materials,[34] produces magnetic scattering for weakly localized carriers.[35]

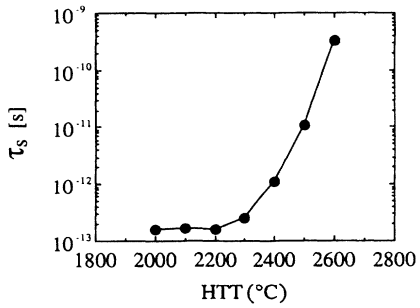

FIG. 9. HTT dependence of the magnetic impurity scattering time τ_s. It is constant for $T_{HT} \leq 2200$ °C, and increases drastically when the HTT is increases, suggesting that magnetic impurities diffuse out of the sample.

F. Final remarks

The theoretical relations for weak localization used in the present work have been derived in the weak disorder limit, i.e., for $k_F l > 1$, where k_F is the Fermi wave vector and l the mean free path of the carriers. Estimating the product $k_F l$ for our samples, we find that $k_F l$ is higher than unity for $T_{HT} \geq 2100$ °C, while for the sample heat treated at 2000 °C, $k_F l$ is lower but close to 1. When the weak-disorder condition is not verified, higher-order terms cannot be neglected and the relations used here are no longer strictly valid.[2] That is the reason why we limited our investigations to samples heat treated at 2000 °C and above.

In most of the 2D electronic systems exhibiting weak-localization effect, the magnitude of the additional resisitivity is generally very small compared to the classical Boltzmann contribution. In contrast, in mainly turbostratic carbons, weak localization contributes to a much larger extent ($\approx 30\%$) to the resistivity at liquid-helium temperature. As stated above, the magnitude of the weak-localization effect is proportional to the sheet resistance $R_\square$ which is found to be much larger in our samples than in the other 2D electronic systems. It is worth noting that as for inversion layers and acceptor GIC's, the mean free path is not limited by the thickness of the 2D layer since it is intrinsically two-dimensional. Pregraphitic materials appear to be well suited to study weak-localization effects in transport properties for which large amplitudes are needed to be observable.

V. CONCLUSIONS

Magnetoresistance and resistivity measurements as well as x-ray-diffraction structural analysis have been performed on a set of pyrocarbon samples heat treated in the temperature range between 2000 and 2600 °C.

The magnetoresistance is negative at least at low temperature and low magnetic field. The amplitude of the effect is rather similar for the samples heat treated at 2000, 2100, and 2200 °C, while it vanishes progressively as the heat-treatment temperature exceeds 2300 °C. Moreover, as previously pointed out in a recent study performed on pregraphitic carbon fibers, the resistivity exhibits an anomalous behavior at low temperature which cannot be explained by simply invoking a thermal

excitation of free carriers.

X-ray structural analysis reveals that a turbostratic-to-graphitic transition occurs when the HTT is raised above 2200 °C.

The whole set of magnetoresistance data is analyzed within the framework of the weak-localization theory for 2D electronic systems. The theoretical relations reproduce the experimental data fairly well. Moreover, the striking low-temperature dependence of the resistivity is simply understood as resulting from the sum of two contributions: the weak-localization contribution, which causes the observed anomalous behavior at low temperature, and the classical Boltzmann contribution. The temperature dependence of the so-called Boltzmann resistivity is qualitatively understood invoking the temperature dependences of both the mobility and free-carrier density.

The 2D behavior is ascribed to the turbostratic structure. More precisely, our results can be understood if it is assumed that only the turbostratic graphene layers exhibit a 2D behavior as far as the weak-localization is concerned, while the graphitic regions do not. X-ray analysis shows that a partially graphitic sample is composed of a mixture of two phases. The first consists of graphitic 3D-ordered stacking sequences, while the second consists of turbostratic layer planes. As HTT increases, the graphitic regions grow to the detriment of turbostratic regions, leading to a vanishing 2D weak-localization effect. The disappearance of the negative magnetoresistance effect as the sample becomes more graphitic is consistent with this kind of 2D-to-3D crossover.

Our results also show that magnetic impurities are present in our samples and that their concentration decreases significantly when the HTT rises above 2300 °C. This observation is in agreement with other investigations which show that impurities diffuse out of partially graphitic samples in the same HTT range.

ACKNOWLEDGMENTS

The authors are indebted to Professor M. S. Dresselhaus for enlightening discussion and critical reading of the manuscript. The work performed in Louvain-la-Neuve was part of the programme "Action de Recherche Concertée" sponsored by the Belgian State (Ministry of Scientific Policy). The cooperation between the Université de Nancy and Université Catholique de Louvain groups was stimulated by travel grants from Centre National de la Recherche Scientifique (France) and CGRI (Belgium). One of us (V.B.) was supported by a grant from the Institut pour l'Encouragement de la Recherche Scientifique dans l'Industrie et l'Agriculture (IRSIA) and another (L.P.) by Fonds National Belge de la Recherche Scientifique.

APPENDIX A

The relations of magnetoresistance given in the text are strictly valid only when the magnetic field direction is perpendicular to the 2D carrier system which lies here in the graphene layers. Since the mosaic spread cannot be neglected in our samples, the observed magnetoresistance is not directly given by relations (2), (5), (6), and (7). According to the large anisotropy of the magnetoresistance in pregraphitic materials,[16] we can assume that only the magnetic field component perpendicular to the graphite layers produces the magnetoresistance. Hence, the apparent magnetoresistance, i.e., the experimental magnetoresistance $[\Delta R(H,T)/R(0,T)]_{\text{expt}}$ is given by[7]

$$\left[\frac{\Delta R(H,T)}{R(0,T)}\right]_{\text{expt}} = \frac{1}{\pi}\int_{-\pi/2}^{\pi/2} f(\theta)\left[\frac{\Delta R(H\cos\theta,T)}{R(0,T)}\right]_{\text{theor}} d\theta\,, \quad \text{(A1)}$$

where θ is the angle between the normal to a graphene layer and the magnetic field direction. The theoretical magnetoresistance which appears under the integral is the one that would be observed if the magnetic field was perpendicular to each graphene layer. We assume that the weight function $f(\theta)$ takes the form of a Gaussian function:

$$f(\theta)=\frac{1}{\sigma\sqrt{2\pi}}\exp\left[-\frac{\theta^2}{2\sigma^2}\right], \quad \text{(A2)}$$

where σ is the standard deviation which has been determined via x-ray experiments.

APPENDIX B

For the less graphitic samples, taking a mean value for $\mu_0 \approx 1.5\times10^{-1}$ m^2/V s and $m^*/m_0=0.012$, we find $\tau_0 \approx 10^{-14}$ s. Taking $v_F=10^6$ m/s, it follows that $D\approx 5\times10^{-3}$ m^2/s. As the graphitization process progresses, it is more difficult to estimate D. However, v_F and τ_0, respectively, decrease and increase as the sample becomes more and more ordered.[15] Therefore, we will make the assumption that D does not depend significantly on HTT, in comparison to the strong dependence of H_s. The weak HTT dependence of α supports that assumption.

[1] E. Abrahams, P. W. Anderson, D. C. Licciardello, and T. V. Ramakrishnan, Phys. Rev. Lett. **42**, 613 (1979).

[2] G. Bergmann, Phys. Rep. **107**, 1 (1984).

[3] P. A. Lee and T. V. Ramakrishnan, Rev. Mod. Phys. **57**, 287 (1985).

[4] S. Hikami, A. I. Larkin, and Y. Nagaoka, Prog. Theor. Phys. **63**, 707 (1980).

[5] *Localization, Interaction and Transport Phenomena,* Vol. 61 of *Springer Series in Solid-State Sciences,* edited by B. Kramer, G. Bergmann, and Y. Bruynseraede (Springer-Verlag, Berlin, 1985).

[6] L. Piraux, J.-P. Issi, J.-P. Michenaud, E. McRae, and J. F. Marêché, Solid State Commun. **56**, 567 (1985); L. Piraux, V. Bayot, J.-P. Michenaud, J.-P. Issi, J. F. Marêché, and E.

McRae, *ibid.* **59**, 711 (1986).
[7]L. Piraux, V. Bayot, X. Gonze, J.-P. Michenaud, and J.-P. Issi, Phys. Rev. B **36**, 9045 (1987).
[8]L. Piraux, V. Bayot, J.-P. Issi, M. S. Dresselhaus, M. Endo, and T. Nakajima, Phys. Rev. B **41**, 4961 (1990).
[9]M. S. Dresselhaus and G. Dresselhaus, Adv. Phys. **30**, 139 (1981).
[10]S. Mrozowski and A. Chaberski, Phys. Rev. **104**, 74 (1956).
[11]Y. Hishiyama, Carbon **8**, 259 (1970).
[12]Y. Hishiyama, A. Ono, and M. Hashimoto, Jpn. J. Appl. Phys. **10**, 416 (1971).
[13]P. Delhaes, P. de Kepper, and M. Uhlrich, Philos. Mag. **29**, 1301 (1974).
[14]R. E. Franklin, Acta Cryst. **4**, 253 (1951).
[15]I. L. Spain, K. J. Volin, H. A. Goldberg, and I. Kalnin, J. Phys. Chem. Solids **44**, 839 (1983).
[16]K. Yazawa, J. Phys. Soc. Jpn. **26**, 1407 (1969).
[17]A. A. Bright, Phys. Rev. B **20**, 5142 (1979).
[18]P. R. Wallace, Phys. Rev. **71**, 622 (1947).
[19]J. W. McClure, Phys. Rev. **104**, 666 (1956).
[20]P. D. Hambourger, Appl. Phys. Commun. **5**(4), 223 (1985).
[21]I. Rahim, K. Sugihara, M. S. Dresselhaus, and J. Heremans, Carbon **24**, 663 (1986).
[22]V. Bayot, L. Piraux, J.-P. Michenaud, and J.-P. Issi, Phys. Rev. B **40**, 3514 (1989).
[23]A. Klein, J. Appl. Phys. **35**, 2947 (1964).
[24]M. S. Dresselhaus, G. Dresselhaus, K. Sugihara, I. L. Spain, and H. A. Goldberg, *Graphite Fibers and Filaments,* Vol. 5 of *Springer Series in Materials Science* (Springer-Verlag, Berlin, 1988).
[25]J. Heremans, Carbon **23**, 431 (1985).
[26]A. Plançon, F. Rousseaux, D. Tchoubar, C. Tchoubar, G. Krinari, and V. A. Drits, J. Appl. Cryst. **15**, 509 (1982).
[27]W. Ruland, *Chemistry and Physics of Carbon,* edited by P. L. Walker Jr. and P. A. Thrower (Dekker, New York, 1968), Vol. 4.
[28]M. Inagaki, Y. Komatsu, and J. V. Zanchetta, Carbon 7, 163 (1969).
[29]R. Rosenbaum, Phys. Rev. B **32**, 2190 (1985).
[30]L. D. Woolf, J. Chin, Y. R. Lin-Liu, and H. Ikezi, Phys. Rev. B **30**, 861 (1984).
[31]I. L. Spain, *Chemistry and Physics of Carbon,* edited by P. L. Walker Jr. and P. A. Thrower (Dekker, New York, 1981), Vol. 16.
[32]M. Gijs, C. Van Haesendonck, and Y. Bruynseraede, J. Phys. F. **16**, 1227 (1986).
[33]B. S. Elman, G. Braunstein, M. S. Dresselhaus, and T. Venkatesan, Nucl. Instrum. Methods, Phys. Res. B **7/8**, 493 (1984).
[34]J. Maire, R. Gremion, M. Moreau, J. Rappeneau, M. Yvars, and A. Fillatre, Carbon **5**, 575 (1967).
[35]G. Bergmann, Phys. Rev. Lett. **49**, 162 (1982).